

PAPER

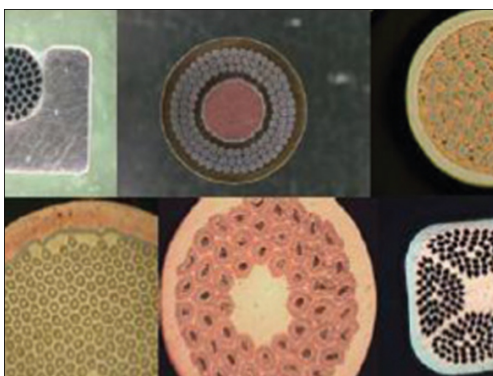
## Vortex pinning properties and microstructure of MgB<sub>2</sub> heavily doped with titanium group elements

To cite this article: Yuhei Takahashi *et al* 2017 *Supercond. Sci. Technol.* **30** 125006

View the [article online](#) for updates and enhancements.

### Related content

- [Optimization of vortex pinning at grain boundaries on ex-situ MgB<sub>2</sub> bulks synthesized by spark plasma sintering](#)  
Tomoyuki Naito, Yuri Endo and Hiroyuki Fujishiro
- [Ti-doping effects on magnetic properties of dense MgB<sub>2</sub> bulk superconductors](#)  
Tomoyuki Naito, Takafumi Yoshida and Hiroyuki Fujishiro
- [Potential ability of 3 T-class trapped field on MgB<sub>2</sub> bulk surface synthesized by infiltration-capsule method](#)  
Tomoyuki Naito, Arata Ogino and Hiroyuki Fujishiro



## **SUPERCON, Inc.**

### **Superconducting Wire and Cable**

**Standard and Speciality designs are available to meet your most demanding superconductor requirements.**

SUPERCON, Inc. has been producing niobium-based superconducting wires and cables for half a century. We are the original SUPERCON - the world's first commercial producer of niobium-alloy based wire and cable for superconducting applications.

**“We deliver superconductivity!”**

**[www.SUPERCON-WIRE.com](http://www.SUPERCON-WIRE.com)**

# Vortex pinning properties and microstructure of MgB<sub>2</sub> heavily doped with titanium group elements

Yuhei Takahashi, Tomoyuki Naito  and Hiroyuki Fujishiro

Faculty of Science and Engineering, Iwate University, Morioka 020-8551, Japan

E-mail: [tnaito@iwate-u.ac.jp](mailto:tnaito@iwate-u.ac.jp)

Received 9 August 2017, revised 27 September 2017

Accepted for publication 9 October 2017

Published 1 November 2017



CrossMark

## Abstract

The doping of titanium group elements (TGE; Ti, Zr, Hf) to MgB<sub>2</sub> is known to improve vortex pinning properties. However, the optimal doping level of each TGE is still a controversial issue. In this study, to improve the critical current density,  $J_c$ , in high magnetic-field by the TGE-doping, we have studied the vortex pinning properties of (Mg<sub>1-x</sub>TGE<sub>x</sub>)B<sub>2</sub> samples with  $x$  ranging in the interval  $0 < x < 0.5$ . The  $J_c$  of 1.2 kA cm<sup>-2</sup> at 20 K in 3 T for the pristine sample was maximized to 2.9 kA cm<sup>-2</sup> for the Ti20%-doped sample, 4.9 kA cm<sup>-2</sup> for the Zr30%-doped one, and 5.2 kA cm<sup>-2</sup> for the Hf30%-doped one under identical temperature and magnetic field. The irreversibility field,  $\mu_0 H_{irr}$ , of 3.8 T for the pristine sample was also shifted to a higher field of 4.2 T, 4.3 T and 4.6 T by the Ti20%-, Zr30%- and Hf30%-doping, respectively. Microstructural observations suggested that the grain size, shape and distribution of the MgB<sub>2</sub> and impurity phases depended strongly on the species of TGE. We discuss the mechanism of the enhanced vortex pinning properties of the TGE-doped MgB<sub>2</sub>.

Keywords: MgB<sub>2</sub>, critical current density, titanium group elements, doping effects

(Some figures may appear in colour only in the online journal)

## 1. Introduction

The MgB<sub>2</sub> superconductor with the critical temperature,  $T_c$ , of 39 K [1] can be operated at liquid hydrogen temperature. No weak coupling between the MgB<sub>2</sub> grains [2, 3] enables an untextured sample with high critical current density,  $J_c$ , over 10<sup>5</sup> A cm<sup>-2</sup> at 20 K in the self-field [4]. However, the  $J_c$  value of MgB<sub>2</sub> is known to strongly deteriorate in magnetic fields [4], which must be improved for practical superconducting wire and bulk applications such as a magnet [5–8], motor [9] and generator [10]. Chemical doping or substitution is one of the solutions to improve the vortex pinning properties of MgB<sub>2</sub>. Substituting carbon (C), derived from various carbon sources including SiC [11], B<sub>4</sub>C [12], the fullerene (C<sub>60</sub>) [13], carbohydrates [14] and so on, for the B-site enhances the upper critical field,  $\mu_0 H_{c2}$ , by shortening the coherence length, resulting in the highly enhanced  $J_c$  in higher magnetic-fields. In addition to the carbon, the doping of titanium group elements (TGE; Ti, Zr, Hf) also significantly improved the

$J_c$ -properties of MgB<sub>2</sub> under high magnetic fields [8, 15–19], in which the optimal TGE-doping level of 1%–20% depended on the species of TGE. The pioneering work, which examined the Ti-doping effects, showed that the three orders magnitude larger  $J_c$  was achieved for the Ti10%-doped MgB<sub>2</sub> sample compared to that of the non-doped one [15]. Furthermore, the Zr-doping also offered the enhanced  $J_c$  characteristics [17]. The optimal Ti- and Zr-doping level of 10% was found in the literatures [15, 17, 19]. Goto *et al* claimed that the Zr- and Hf-doping were more effective to enhance the  $J_c$ -properties than the Ti-doping and obtained the maximized  $J_c$  at the doping level of 1%–2% [18]. However, the doping level dependence of the  $J_c$ ,  $J_c(x)$ , suggested that the higher  $J_c$  might be obtained for the higher  $x$  than 10%. We also found that both  $J_c$  and the trapped field,  $B_T$ , of Ti-doped MgB<sub>2</sub> bulks were enhanced up to the Ti-doping level of 20% [8, 20]. In the Ti-doped MgB<sub>2</sub>, a non-superconductive TiB<sub>2</sub> thin layer was created at the boundary of MgB<sub>2</sub> grains, and then suppressed the grain growth of MgB<sub>2</sub> without the disturbance of supercurrent

flowing [16]. On the other hand, the microscopic analysis for the Zr- and Hf-doped  $\text{MgB}_2$  to clarify the pinning mechanism has not been carried out yet. Consequently, the optimal doping level of each TGE and the pinning mechanism of the Zr- and Hf-doped  $\text{MgB}_2$  are still controversial issues to date. In this paper, we studied the vortex pinning properties of the  $\text{MgB}_2$  samples heavily doped with TGE (Ti, Zr, Hf) up to 50% and discussed the pinning mechanism for the heavily doped region.

## 2. Experimental details

### 2.1. Fabrication of $\text{MgB}_2$ samples

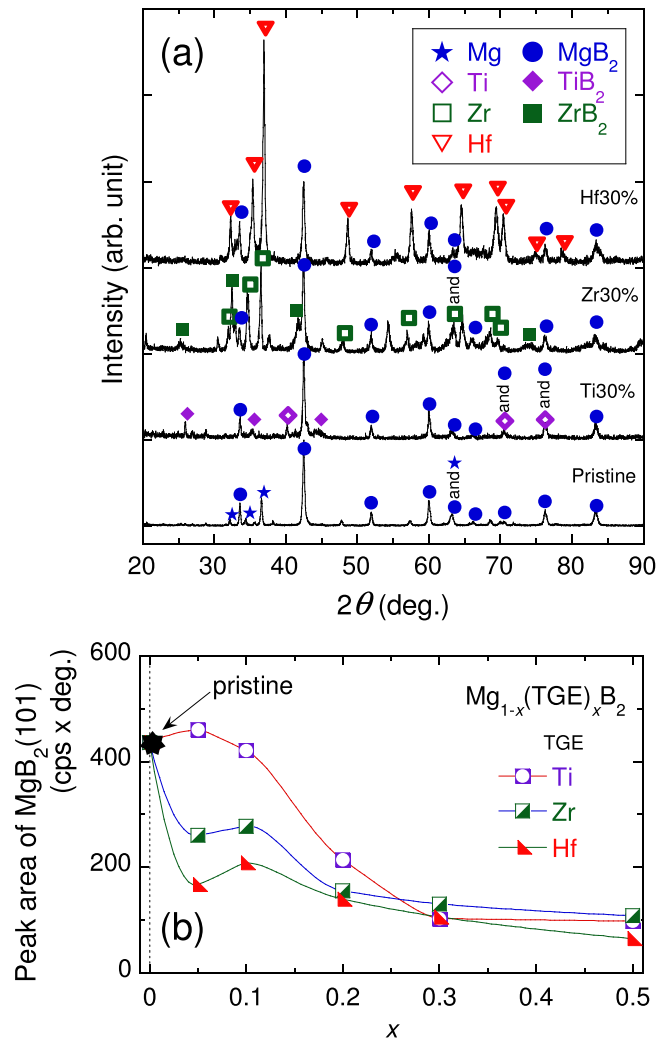
$(\text{Mg}_{1-x}\text{TGE}_x)\text{B}_2$  sample was fabricated by a conventional *in-situ* powder-in-closed-tube method. Raw powders with 99% in purity of Mg ( $\leq 180 \mu\text{m}$  in grain size, Kojundo Chemical Laboratory Co., Ltd), amorphous B ( $\leq 46 \mu\text{m}$  in grain size, Furuuchi Chemical Co.), Ti ( $\leq 45 \mu\text{m}$  in grain size, Furuuchi Chemical Co.), Zr ( $\leq 61 \mu\text{m}$  in grain size, Furuuchi Chemical Co.) and Hf ( $\leq 50 \mu\text{m}$  in grain size, Furuuchi Chemical Co.) were weighed with  $\text{Mg}:\text{TGE}:\text{B} = (1.1-x):x:2.0$  in molar ratio and mixed by agate motor and pestle for 1 h. Well-mixed powder was poured into a closed-end stainless steel (SUS) tube with 6 and 5 mm in outer and inner diameters, respectively, pressed into the tube using a SUS rod, and the other end of SUS tube was closed by pressing. Subsequently, the main body was pressed into a plate, and finally both ends were bent at  $180^\circ$ . The precursor in the closed tube was sintered at  $800^\circ\text{C}$  for 1 h in 0.1 MPa flowing Ar in a tube furnace. The relative density was estimated to be about 50% of the ideal density for all the samples.

### 2.2. Measurements

The constituent phase and structure of  $(\text{Mg}_{1-x}\text{TGE}_x)\text{B}_2$  sample were evaluated by the x-ray diffraction using the  $\text{Cu-K}\alpha$  radiation (the wave length of 0.154 nm) operated with the acceleration voltage of 30 kV and electron current of 30 mA. Temperature and magnetic-field dependences of magnetization,  $M(T)$  and  $M(\mu_0 H)$ , were measured by a commercial SQUID magnetometer (MPMS-XL, Quantum Design Inc.). Critical current density,  $J_c$ , was estimated from the magnetic hysteresis loop,  $M(\mu_0 H)$ , using the extended Bean's critical state model [21, 22]. Microstructural observation and analysis of chemical composition were performed by a scanning electron microscopy with a field emission electron gun (FE-SEM; JSM-7001F, JEOL Ltd.), coupled with energy dispersive x-ray spectroscopy and electron backscatter diffraction (EBSD; NordlysNano, Oxford Instruments plc).

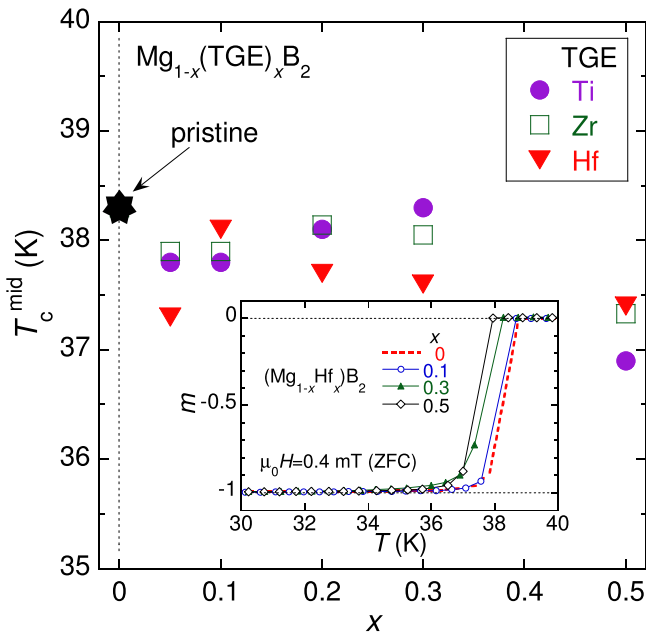
## 3. Results and discussion

Figure 1(a) shows the typical XRD patterns for the pristine and TGE30%-doped  $\text{MgB}_2$  samples. The main phase of the pristine sample was  $\text{MgB}_2$  with a small amount of residual



**Figure 1.** (a) Powder x-ray diffraction patterns for the pristine and TGE30%-doped  $\text{MgB}_2$  samples. (b) The peak area of  $\text{MgB}_2(101)$  peak as a function of the TGE-doping content,  $x$ . The lines are guides to the eye.

Mg. For the Ti30%-doped sample, the main phase was  $\text{MgB}_2$  with a small amount of residual Ti and created  $\text{TiB}_2$ . For the Zr30%- and Hf30%-doped samples, the  $\text{MgB}_2$  phase was confirmed, but quite a large amount of impurities appeared. The Zr30%-doped sample contained both Zr and  $\text{ZrB}_2$  impurities. Unreacted Hf metal appeared as the impurity for the Hf30%-doped sample. In addition, no peak shift of the  $\text{MgB}_2$  phase by the TGE-doping was observed, suggesting that the Mg-site substitution by the TGE did not occur. Figure 1(b) shows the peak area of  $\text{MgB}_2(101)$  versus the TGE-doping content,  $x$ , for the  $(\text{Mg}_{1-x}\text{TGE}_x)\text{B}_2$  samples. The peak area of the Ti-doped samples was almost independent of  $x$  for  $x \leq 0.1$ , and decreased monotonically with increasing  $x$ . On the other hand, the steep decrease in the peak area with  $x$  was observed for both Zr- and Hf-doped samples, and was almost the same among three TGE-doped samples above  $x = 0.3$ . The reduction rate was obviously larger than that expected from the volume fraction of  $\text{MgB}_2$ , assuming the same amounts and crystallinity of the  $\text{MgB}_2$  phase for all the samples. In other word, a part of the  $\text{MgB}_2$  phase was



**Figure 2.** Critical temperature defined at the midpoint,  $T_c^{\text{mid}}$ , as a function of the TGE-doping content,  $x$ . Inset shows the temperature dependence of the normalized magnetization,  $m(T)$  ( $=M(T)/M(10\text{ K})$ ), in a magnetic-field of  $\mu_0 H = 0.4\text{ mT}$  after zero-field cooling for the Hf-doped  $\text{MgB}_2$  samples for various  $x$  values.

distorted by the TGE-doping, which might offer the weak-superconductivity regions acting as pinning centers [23].

Inset of figure 2 shows the temperature dependence of the normalized magnetization,  $m(T)$  ( $=M(T)/M(10\text{ K})$ ), in a magnetic-field of  $\mu_0 H = 0.4\text{ mT}$  after zero-field cooling for the Hf-doped  $\text{MgB}_2$  samples with  $x = 0, 0.1, 0.3$  and  $0.5$ . The Ti- and Zr-doped samples also showed the sharp superconducting transition around 37–38 K (not shown here). The transition temperature,  $T_c^{\text{mid}}$ , defined at the midpoint of the transition, was plotted as a function of  $x$ , in the main panel of figure 2. Although the  $T_c^{\text{mid}}$  was almost insensitive to the TGE-doping level, some TGE-doped samples showed somewhat lower  $T_c^{\text{mid}}$  than the pristine sample. The  $T_c$ -reduction possibly originated from the introduction of lattice distortion and/or the Mg-site substitution by the TGEs. The former scenario of the introduction of distortion in the  $\text{MgB}_2$  crystal is preferable, because the deformed crystal generally degrades the superconductivity [24]. The latter scenario of the site substitution can be discarded here, because no XRD peak shift of the  $\text{MgB}_2$  phase by the TGE-doping was observed, as described in the preceding paragraph. Furthermore, the similar  $x$ -independent  $T_c^{\text{mid}}(x)$  behavior was also reported previously for the TGE-doped  $\text{MgB}_2$  bulk prepared by a HIP method [18, 20]; the authors also claimed no solid solution between Mg and Ti.

Figure 3(a) shows the magnetic-field dependence of the critical current density,  $J_c(\mu_0 H)$ , at 20 K for the pristine and TGE30%-doped samples. For the pristine sample, the  $J_c$  of about  $0.9 \times 10^5\text{ A cm}^{-2}$  in the self-field decreased steeply with increasing magnetic-field and reached to  $100\text{ A cm}^{-2}$  at  $\mu_0 H = 3.8\text{ T}$ , which was defined as the irreversibility field,

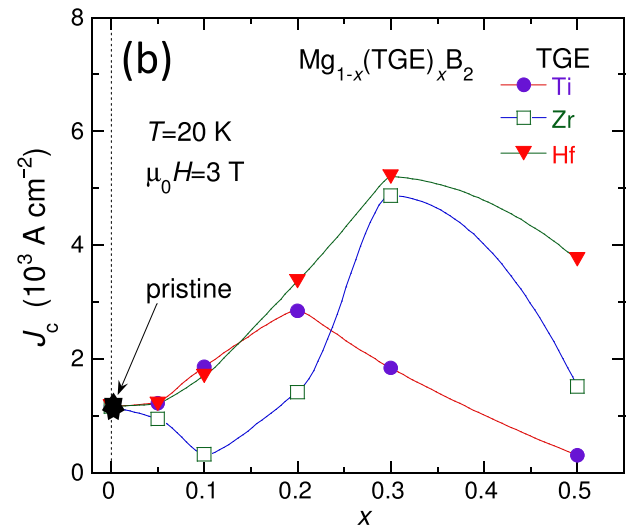
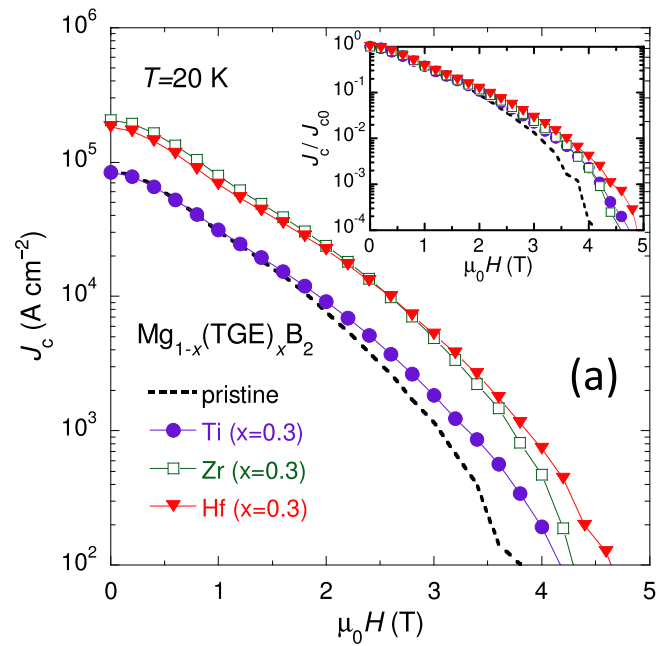


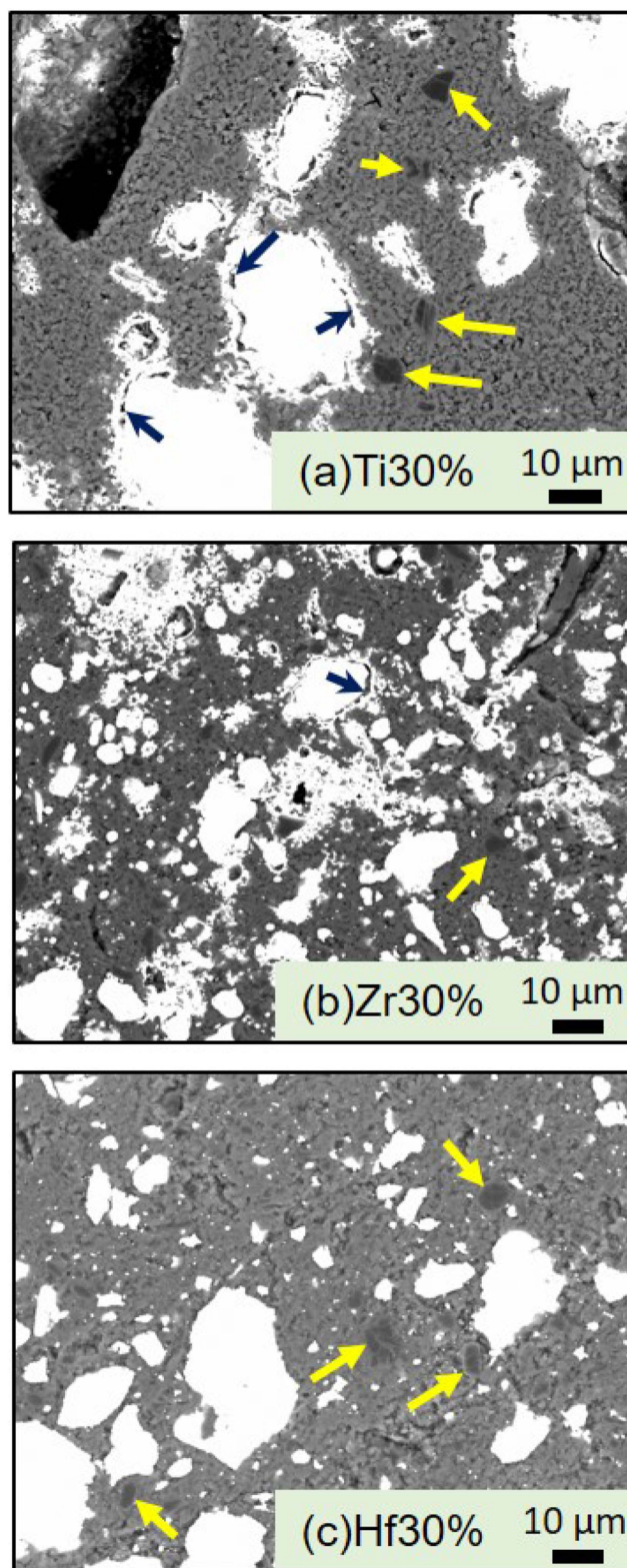
**Figure 3.** (a) Magnetic-field dependence of the critical current density,  $J_c(\mu_0 H)$ , at 20 K for the pristine and TGE30%-doped samples. Inset shows the magnetic-field dependent  $J_c$  normalized by the self-field  $J_c, J_c/J_{c0}$ . (b) The  $J_c$ s in  $\mu_0 H = 3\text{ T}$  at 20 K as a function of the TGE-doping content,  $x$ , for the TGE-doped  $\text{MgB}_2$  samples. The lines are guides to the eye.

$\mu_0 H_{\text{irr}}$ . The  $J_c(\mu_0 H)$  was enhanced clearly by the TGE-doping and the irreversibility field,  $\mu_0 H_{\text{irr}}$  of 3.8 T for the pristine sample was also shifted to higher field of 4.2 T, 4.3 T and 4.6 T by Ti30%-, Zr30%- and Hf30%-doping, respectively. Inset of figure 3(a) shows the magnetic-field dependent normalized  $J_c, J_c/J_{c0}$ , where  $J_{c0}$  is the self-field  $J_c$ . The  $J_c/J_{c0}$  of the TGE-doped samples started to deviate evidently from that of the non-doped one above around 2 T and showed higher  $J_c/J_{c0}$  and  $\mu_0 H_{\text{irr}}$ . This indicates that the TGE-doping introduced the pinning centers acting effectively at high fields, especially for the Hf-doping. Figure 3(b) shows the  $J_c$ s at 20 K in  $\mu_0 H = 3\text{ T}$  as a function of TGE-doping content,  $x$ . The  $J_c$  of  $1.2 \times 10^3\text{ A cm}^{-2}$  for the pristine sample was

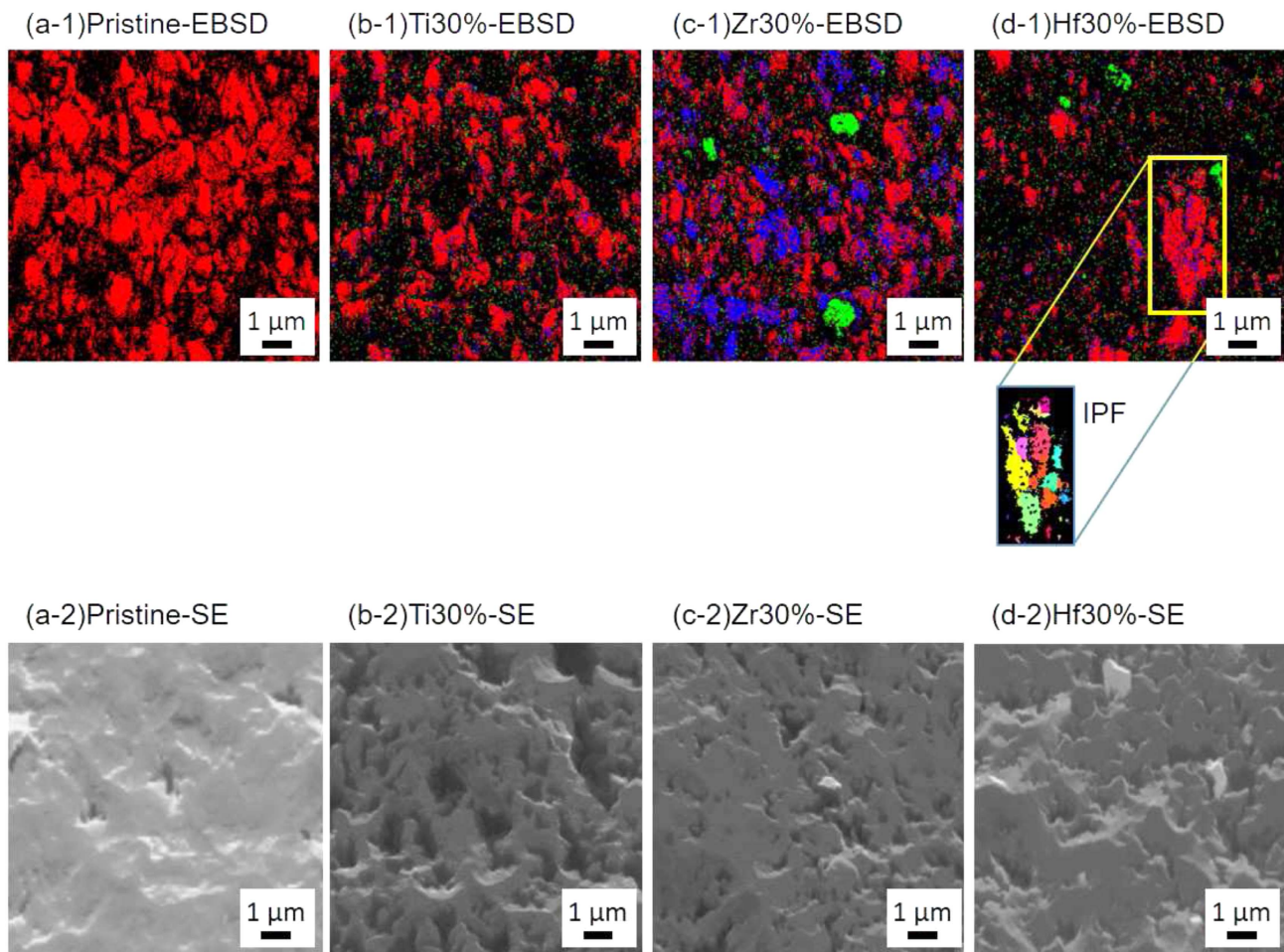
evidently maximized to  $2.9 \times 10^3 \text{ A cm}^{-2}$  for the Ti20%-doped sample,  $4.9 \times 10^3 \text{ A cm}^{-2}$  for the Zr30%-doped one, and  $5.2 \times 10^3 \text{ A cm}^{-2}$  for the Hf30%-doped one. The optimal doping level of 30% for both Zr and Hf is quite higher than the reported values below 10% [17, 18]. The  $J_c$ -peak values of both Zr- and Hf-doped samples were nearly comparable, but the  $x$  dependence of  $J_c$  for the Hf-doped samples was moderate. Furthermore, the  $J_c$  for the Zr50%- and Hf50%-doped sample was still higher than the  $J_c$  of the pristine sample. The  $J_c$ -peak comes from the competition among various factors of the number density of pinning centers, the connectivity [25], the  $\text{MgB}_2$  volume fraction, the crystallinity of  $\text{MgB}_2$  and so on, because the literatures revealed that the TGE-doping offered the fine and well-connected  $\text{MgB}_2$  grains [15, 16, 20, 26]. We suggest that the Hf-doping more effectively suppresses the grain growth and aids the sintering than the Ti- and Zr-doping.

Figure 4 shows the backscattered electron (BSE; compositional contrast) images for the Ti30%-, Zr30%- and Hf30%-doped  $\text{MgB}_2$  samples. Bright and dark gray regions existed in the light gray matrix. The quantitative EDS analysis revealed that the bright, dark gray and light gray regions were unreacted TGE,  $\text{MgB}_4$  and  $\text{MgB}_2$ , respectively. The periphery of some bright region containing a streak, which was indicated by black arrows, was determined to be  $(\text{TGE})\text{B}_2$  for the Ti30%- and Zr30%-doped samples.  $\text{HfB}_2$  region was not confirmed around the Hf precipitates for the Hf30%-doped sample, which is consistent with no  $\text{HfB}_2$  peak in the XRD pattern shown in figure 1(a). The size of Zr-based particles was rather smaller than that of Ti- and Hf-based ones, regardless of the grain size of as-manufactured powders.

Figure 5 shows the EBSD and the secondary electron (SE) images for the pristine and TGE30%-doped  $\text{MgB}_2$  samples. The incident electron beam inclined by  $20^\circ$  from the sample surface was focused on the matrix. The EBSD analysis was applied for the  $\text{MgB}_2$ ,  $(\text{TGE})\text{B}_2$  and TGE crystals, which were represented by red, blue and green colors, respectively. The voids, the residual Mg (not analyzed here) and the fine crystal smaller than the resolution limit of present EBSD device of 50 nm possibly existed in the unanalyzed black area. The volume fraction of examined compounds and elements, which were estimated from the EBSD results, are summarized in table 1. Only the red  $\text{MgB}_2$  and unanalyzed black areas were observed in the pristine sample shown in figure 5(a-1). The residual Mg, which was confirmed by the XRD, should exist in the unanalyzed black area, as reported previously [27]. In addition to both  $\text{MgB}_2$  and unanalyzed areas, some impurities found in the XRD patterns were detected for the Zr30%- and Hf30%-doped samples. Both Zr and  $\text{ZrB}_2$  particles were clearly observed for the Zr30%-doped sample (figure 5(c-1)). For the Hf30%-doped sample, a few nanometric Hf particles was observed but  $\text{HfB}_2$  did not exist in the EBSD image (figure 5(d-1)). On the other hand, for the Ti30%-doped sample, both Ti and  $\text{TiB}_2$  were not found in the EBSD image (figure 5(b-1)), although the existence of both phases was confirmed by the XRD patterns (figure 1(a)) and the BSE image accompanied with the EDS analysis (figure 4(a)). Since the incident electron beam was



**Figure 4.** Backscattered electron (compositional contrast) images for the (a) Ti30%-, (b) Zr30%- and (c) Hf30%-doped  $\text{MgB}_2$  samples. Yellow and black arrows indicate a dark gray area and a streak in a bright area, respectively (see text).



**Figure 5.** EBSD and SE images for the (a) pristine and (b) Ti30%-, (c) Zr30%- and (d) Hf30%-doped  $\text{MgB}_2$  samples. For the EBSD images, red is  $\text{MgB}_2$ , blue is  $(\text{TGE})\text{B}_2$ , green is TGE and black is unanalyzed areas (see text). An IPF plot for the Hf30%-doped sample is shown.

**Table 1.** Volume fraction of compounds and elements in the pristine and TGE30%-doped  $\text{MgB}_2$  bulks.

Sample	Composition of analyzed compounds and elements (%)			
	$\text{MgB}_2$	$(\text{TGE})\text{B}_2$	TGE	Unanalyzed
Pristine	44	–	–	56
Ti30%-doped	25	4	4	67
Zr30%-doped	24	14	5	57
Hf30%-doped	15	4	4	77

focused on the matrix avoiding the visible impurities, the large Ti precipitates with  $\text{TiB}_2$ , as found in figure 4(a), were not naturally detected by the EBSD. The EBSD image for the Ti30%-doped sample suggests strongly the absence of any small nanometric Ti particles in the matrix.  $\text{TiB}_2$  possibly existed as a lamellar between the  $\text{MgB}_2$  grains [16], the size of which was naturally smaller than the present EBSD resolution limit of about 50 nm. We note that the  $\text{ZrB}_2$  thin layers [17] also probably exist in addition to the  $\text{ZrB}_2$  grains. As

found in the EBSD images (figures 5(a-1, b-1, c-1, d-1)), the size of observable  $\text{MgB}_2$  grains decreased and the unanalyzed area increased by the TGE-doping. Somewhat large  $\text{MgB}_2$  grains are confirmed to be assembly of nanometric  $\text{MgB}_2$  grains having different crystal orientation by an inverse pole figure plot (IPF), as shown typically for the Hf30%-doped sample. The SE images (figures 5(a-2, b-2, c-2, d-2)) demonstrate that the volume fraction of voids was rather smaller than that of unanalyzed area, thus the unanalyzed black area originates from not only voids and residual Mg but also fine grains smaller than 50 nm in diameter and/or distorted grains in the matrix. The grain refining and the introduction of distortion are usually confirmed by the broadening of a XRD peak. The full width at half maximum of the  $\text{MgB}_2(101)$  peak increased from  $0.26^\circ$  for the pristine sample to  $0.29^\circ$ ,  $0.38^\circ$  and  $0.35^\circ$  for the Ti30%-, Zr30%- and Hf30%-doped samples, respectively. Therefore, the refined and/or distorted  $\text{MgB}_2$  grains probably exist in the unanalyzed area, and then predominantly enhanced  $J_c$ -properties. The distorted grains should offer the weak-superconductivity regions acting as the field-induced pinning centers, which is consistent with the improved high-field  $J_c$ , as shown in figure 3(a). The volume fraction of  $\text{MgB}_2$  and unanalyzed area for the Hf30%-

doping are rather smaller and larger than those for the Ti30%- and Zr30%-doping. This suggests the larger amount of fine MgB<sub>2</sub> grains in the Hf30%-doped sample, which is one of the possibilities to the dramatically improved  $J_c$ -characteristics in the Hf-doped MgB<sub>2</sub> for the wide range of  $x$ . Although the sub-micron size of impurity particles such as Zr, ZrB<sub>2</sub> and Hf is rather larger than  $2\xi \sim 10$  nm [28] ( $\xi$  is the coherence length), they can act as the pinning centers and contributed slightly the enhancement of  $J_c$ -properties.

Zhao *et al* pointed out that the lamellar TiB<sub>2</sub> region created at the surface of MgB<sub>2</sub> grain suppressed the grain growth of MgB<sub>2</sub> and realized the nanometric MgB<sub>2</sub> grains [16]. The Hf-doping also offered the fine MgB<sub>2</sub> grains regardless of the absence of HfB<sub>2</sub>. The result resembles to our results reported previously [20], in which the Ti-doped MgB<sub>2</sub> bulk without TiB<sub>2</sub> layer offered the nanometric MgB<sub>2</sub> grains. It is noteworthy that the low sintering temperature of 700 °C for the previous Ti-doped MgB<sub>2</sub> might not allow the creation of TiB<sub>2</sub> phase. Our present and previous results suggest that the existence of (TGE)B<sub>2</sub> phase does not necessarily obtain the fine MgB<sub>2</sub> grains. However, the mechanism of grain refining without (TGE)B<sub>2</sub> remains unsolved problem.

#### 4. Summary

We have studied the doping effects of titanium group elements (TGE = Ti, Zr, Hf) on the vortex pinning properties for the (Mg<sub>1-x</sub>TGE<sub>x</sub>)B<sub>2</sub> prepared by a powder-in-closed-tube method. The critical current density,  $J_c$ , of 1.2 kA cm<sup>-2</sup> at 20 K in 3 T for the pristine sample was evidently maximized to 2.9 kA cm<sup>-2</sup> for the Ti20%-doped sample, 4.9 kA cm<sup>-2</sup> for the Zr30%-doped one, and 5.2 kA cm<sup>-2</sup> for the Hf30%-doped one. The irreversibility field,  $\mu_0 H_{irr}$ , of 3.8 T for the pristine sample was also shifted to higher field of 4.2 T, 4.3 T and 4.6 T by Ti20%-, Zr30%- and Hf30%-doping, respectively. The optimal doping levels were  $x = 0.2$  for the Ti-doping and 0.3 for the Zr- and Hf-doping. In addition, the Hf-doping enhanced the  $J_c$  value for a wider Hf-content compared to the Zr-doping. These results suggest that the Hf-doping is the most effective to improve the vortex pinning properties of MgB<sub>2</sub> among TGEs. Microstructural analysis revealed that the TGE-doping offered the fine MgB<sub>2</sub> grains. In particular, the Hf-doping promoted the creation of nanometric MgB<sub>2</sub>, which resulted in the highly improved  $J_c$  and  $\mu_0 H_{irr}$ . Finally, the  $J_c$  of the Zr50%- and Hf50%-doped samples was still higher than that of the pristine one, which suggested that the refining MgB<sub>2</sub> grains were preferable to enhance the  $J_c$ -properties, compared to the volume fraction of MgB<sub>2</sub>.

#### Acknowledgments

The authors would like to thank Drs T Murakami and K Nonaka and Mr K Sasaki of Iwate University for their assistance in microstructural analysis using FE-SEM-EDS/EBSD and FE-EPMA apparatuses. This work was partly

supported by JSPS KAKENHI Grant Numbers JP15K04718, JP15K04646.

#### ORCID iDs

Tomoyuki Naito  <https://orcid.org/0000-0001-7594-3466>

#### References

- [1] Nagamatsu J, Nakagawa N, Muranaka T, Zenitani Y and Akimitsu J 2001 *Nature* **410** 63–4
- [2] Kambara M, Babu N H, Sadki E S, Cooper J R, Minami H, Cardwell D A, Campbell A M and Inoue I H 2001 *Supercond. Sci. Technol.* **14** L5–7
- [3] Larbalestier D C *et al* 2001 *Nature* **410** 186–9
- [4] Bugoslavsky Y, Perkins G K, Qi X, Cohen L F and Caplin A D 2001 *Nature* **410** 563–5
- [5] Ling J, Voccio J P, Hahn S, Qu T, Bascuñán J and Iwasa Y 2017 *Supercond. Sci. Technol.* **30** 024011
- [6] Naito T, Sasaki T and Fujishiro H 2012 *Supercond. Sci. Technol.* **25** 095012
- [7] Yamamoto A, Ishihara A, Tomita M and Kishio K 2014 *Appl. Phys. Lett.* **105** 032601
- [8] Naito T, Yoshida T and Fujishiro H 2015 *Supercond. Sci. Technol.* **28** 095009
- [9] Kajikawa K *et al* 2012 *Cryogenics* **52** 615–9
- [10] Ohsaki H, Terao Y and Sekino M 2010 *J. Phys.: Conf. Ser.* **234** 032043
- [11] Dou S X, Soltanian S, Horvat J, Wang X L, Zhou S H, Ionescu M, Liu H K, Munroe P and Tomsic M 2002 *Appl. Phys. Lett.* **81** 3419–21
- [12] Lezza P, Senatore C and Flükiger R 2006 *Supercond. Sci. Technol.* **19** 1030
- [13] Miu L, Aldica G, Badica P, Ivan I, Miu D and Jakob G 2010 *Supercond. Sci. Technol.* **23** 095002
- [14] Ye S J, Matsumoto A, Zhang Y C and Kumakura H 2014 *Supercond. Sci. Technol.* **27** 085012
- [15] Zhao Y, Feng Y, Cheng C H, Zhou L, Wu Y, Machi T, Fudamoto Y, Koshizuka N and Murakami M 2001 *Appl. Phys. Lett.* **79** 1154–6
- [16] Zhao Y, Huang D X, Feng Y, Cheng C H, Machi T, Koshizuka N and Murakami M 2002 *Appl. Phys. Lett.* **80** 1640–2
- [17] Feng Y, Zhao Y, Pradhan A K, Cheng C H, Yau J K F, Zhou L, Koshizuka N and Murakami M 2002 *J. Appl. Phys.* **92** 2614–9
- [18] Goto D, Machi T, Zhao Y, Koshizuka N, Murakami M and Arai S 2003 *Physica C* **392-396** 272–5
- [19] Prikhna T *et al* 2004 *Physica C* **402** 223–33
- [20] Naito T, Yoshida T, Mochizuki H, Fujishiro H, Basu R and Szpunar J A 2016 *IEEE Trans. Appl. Supercond.* **26** 6800805
- [21] Bean C P 1962 *Phys. Rev. Lett.* **8** 250–3
- [22] Gyorgy E M, van Dover R B, Jackson K A, Schneemeyer L F and Waszczak J V 1989 *Appl. Phys. Lett.* **55** 283–5
- [23] Campbell A and Evetts J 1972 *Adv. Phys.* **21** 199–428
- [24] Naito T, Endo Y and Fujishiro H 2017 *Supercond. Sci. Technol.* **30** 095007
- [25] Rowell J M 2003 *Supercond. Sci. Technol.* **16** R17
- [26] Zhao Y, Feng Y, Huang D, Machi T, Cheng C, Nakao K, Chikumoto N, Fudamoto Y, Koshizuka N and Murakami M 2002 *Physica C* **378-381** 122–6

[27] Ogino A, Naito T and Fujishiro H 2017 *IEEE Trans. Appl. Supercond.* **27** 6800905

[28] Buzea C and Yamashita T 2001 *Supercond. Sci. Technol.* **14** R115